engineering proceedings

MDPI

Proceeding Paper

O.I.C.-Based Design of Aluminum Circular Hollow Sections under Compression or Pure Bending †

Liya Li [1], Sahar Dahboul [2], Prachi Verma [2], Pampa Dey [2], Mario Fafard [3,4] and Nicolas Boissonnade [2,*]

[1] Department of Civil and Building Engineering, Université de Sherbrooke, Québec, QC J1K 2R1, Canada; liya.li@usherbrooke.ca
[2] Department of Civil and Water Engineering, Université Laval, Québec, QC G1V 0A6, Canada; sahar.dahboul.1@ulaval.ca (S.D.); prachi.verma.1@ulaval.ca (P.V.); pampa.dey@gci.ulaval.ca (P.D.)
[3] Aluminium Research Centre—REGAL, Québec, QC G1V 0A6, Canada; mario.fafard@aluquebec.com
[4] AluQuebec, Montréal, QC H3A 1K2, Canada
* Correspondence: nicolas.boissonnade@gci.ulaval.ca
† Presented at the 15th International Aluminium Conference, Québec, QC, Canada, 11–13 October 2023.

Abstract: This paper investigates the ultimate resistance of aluminum circular hollow sections (C.H.S.) under simple load cases as affected by local buckling and material strain hardening. Following the development of advanced non-linear shell finite element models and their validation against existing test data, extensive non-linear numerical analyses were carried out, varying several key parameters such as alloy types, load case (compression or pure bending) and various section dimensions. The numerical results are used as references to analyze the structural performance of aluminum C.H.S., and to assess the accuracy of design equations based on the Overall Interaction Concept (O.I.C.). The O.I.C.-based proposal is shown to yield more accurate, consistent, and continuous resistance predictions than Eurocode 9 recommendations.

Keywords: aluminum; circular hollow sections; local buckling

check for updates

Citation: Li, L.; Dahboul, S.; Verma, P.; Dey, P.; Fafard, M.; Boissonnade, N. O.I.C.-Based Design of Aluminum Circular Hollow Sections under Compression or Pure Bending. *Eng. Proc.* **2023**, *43*, 31. https://doi.org/10.3390/engproc2023043031

Academic Editor: Houshang Alamdari

Published: 19 September 2023

1. Introduction

The increasing adoption of aluminum alloys as a principal structural material in construction has gained significant attention owing to its multitude of advantages. These advantages encompass a remarkable strength-to-weight ratio, exceptional durability, resistance to corrosion, and recyclability [1,2]. Nevertheless, despite its numerous merits, the relatively lower Young's modulus of aluminum alloys often adversely impacts the buckling behavior and ultimate resistance of structural elements made from aluminum. In response to this concern, many researchers have conducted relevant experimental and numerical analyses [3–6]. In particular, for Circular Hollow Section (C.H.S.) members, which are the focus of this study, Zhu and Young [7] conducted bending and beam-column tests on 6061-T6 aluminum alloy fabricated C.H.S. The test results were compared to Eurocode 9 [8,9], to the Aluminum Design Manual (A.D.M.) [10], and to the Australian/New Zealand Standards [11], which were found to be generally conservative. Additionally, they also performed an extensive numerical analysis [12], comparing the results with predictions from the Direct Strength Method (D.S.M.). The analysis demonstrated that the D.S.M. predictions were also conservative for the aluminum C.H.S. columns. Rong et al. [13] tested 16 7A04-T6 extruded CHS aluminum alloy columns under eccentric load. Comparing experimental and numerical results with Eurocode 9 [8,9] predictions, the latter code was found to be conservative for specimens with larger eccentricity but overestimated strength for specimens with smaller eccentricity ratios and longer member lengths. More research on the global stability of aluminum alloy CHS can be found in [4,5,14–16].

However, the local stability of aluminum C.H.S. has received relatively less attention. To address this gap, a recent study by the authors of this study [17] conducted a test

program to investigate the ultimate capacities and failure modes of extruded 6061-T6 C.H.S. aluminum alloy columns under axial compression and eccentric compression. In the current paper, an extensive numerical parametric study has been carried out on the C.H.S sections under axial and eccentric compressions upon validating their finite element models through the experimental observations in [17]. The parametric study considered a wide range of parameters, including various alloy types, section slenderness, and two simple load cases (compression or pure bending). The numerical results are used as references to analyze the structural performance of aluminum C.H.S. and assess the accuracy of original design equations based on the Overall Interaction Concept (O.I.C.). The proposed O.I.C.-based approach demonstrates more accurate, consistent, and continuous resistance predictions compared to existing standards such as Eurocode 9.

2. Numerical Models

2.1. Features of F.E. Models and Validation

Advanced numerical models were developed and validated against a series of experimental results as described in [17] on C.H.S. stub columns and short beam columns, ensuring the suitability of the adopted numerical approach. All numerical results in this paper were obtained using non-linear finite element (F.E.) analyses performed with the ABAQUS software [18]. Geometrically and materially nonlinear analyses with imperfections (G.M.N.I.A.) were conducted using the "Riks method" [18] to simulate the cross-sectional behavior of the CHS under diverse loading scenarios. The general-purpose S4R shell element was utilized, as it has been proven to deliver excellent performance for aluminum C.H.S. [5,12,19]. A finite element mesh size of $0.1\sqrt{Dt}$ [20] was employed for modeling the extruded C.H.S., where D represents the outer diameter and t denotes the thickness.

The measured dimensions, strain–stress relationships, and geometric imperfections were incorporated into the ABAQUS models. Note that the residual stresses in extruded aluminum sections may be disregarded [2]. Therefore, only the influence of initial geometric imperfections was taken into account. A rigid body boundary condition corresponding to a thick end plate was adopted in the numerical models. At one end, the compression load was applied at a reference point, which was coupled to the end section through rigid body conditions, while the longitudinal displacement U_x of the opposite reference point was prevented, as shown in Figure 1a. For the short beam-columns results reported in [17], all members were loaded concentrically through cylindrical roller supports, which allowed bending rotation around *y-y* axis but restrained torsional twist in the end sections. The distance between each roller end and end-section (e_x) was 135.4 mm. Note that in the subsequent parametric studies conducted on the specimens subjected to pure bending, a nodal force M was applied at reference points (see Figure 1b) to create a constant bending moment.

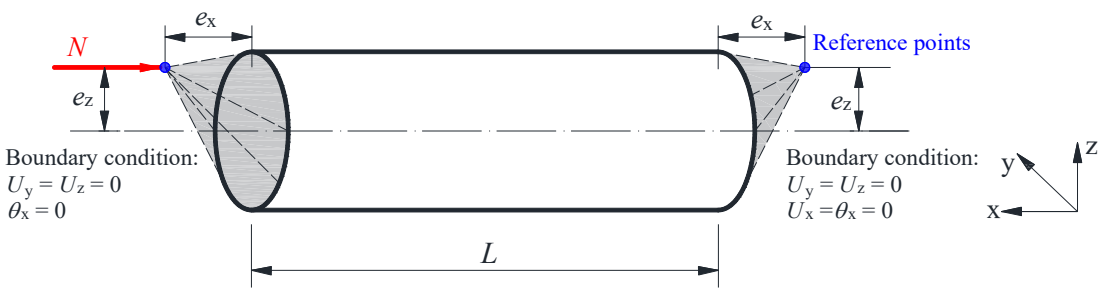

(**a**)

Figure 1. *Cont.*

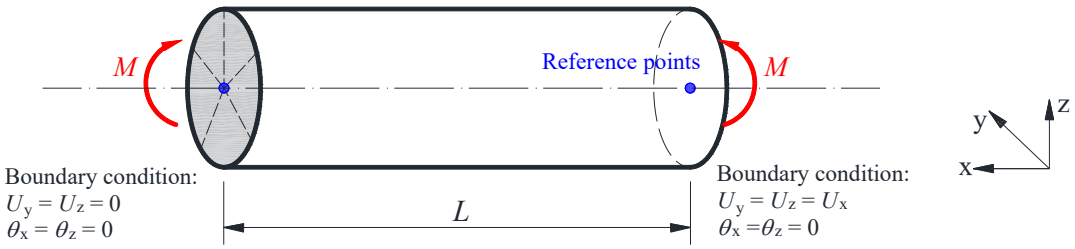

(**b**)

Figure 1. Boundary conditions in numerical models. (**a**) C.H.S. under axial compression or eccentric compression load. (**b**) C.H.S. under pure bending moment *M*.

The numerical results were compared to their corresponding experimental data, and the findings are summarized in Table 1. This table presents the measured values of Young's modulus E and 0.2% proof stress $\sigma_{0.2}$ for these extruded 6061-T6 C.H.S., along with other parameters such as the magnitude of local geometrical imperfection $\omega_{measured}$, the loading eccentricity e_z, the maximum loads recorded during testing $N_{u,Exp.}$ and, in the F.E. simulations, $N_{u,F.E.}$. The ratio of $N_{u,F.E.}/N_{u,Exp.}$ is utilized as an indicator of the performance of the numerical models, as indicated in Table 1. If this ratio is less than 1.0, the numerical resistance prediction is conservative compared to the experimental reference result, and vice versa. Good results are presented for the numerical models, with a mean value equal to 1.05. This indicates that the numerical predictions are within a 3% margin of their corresponding experimental values. Note that in the cases of CHS 6x3/16-e50-BC1 and CHS 6x3/16-e70-BC2, the experimental results were unexpectedly lower than their numerical counterparts. This discrepancy can be attributed to the detachment of the specimen on the tension side from the end plate during the tests, indicating that the boundary condition did not provide sufficient support. As a result, these two cases will be excluded from future analysis. Furthermore, the coefficient of variation (C.O.V.) is as low as 0.05, demonstrating the remarkable ability of the F.E. models to accurately capture and predict the behavior and resistance of the sections.

Table 1. Section geometries and test results for C.H.S. short columns.

Cross-Section	E [MPa]	$\sigma_{0.2}$ [MPa]	D [mm]	t [mm]	L [mm]	$\omega_{measured}$ [mm]	e_z [mm]	$N_{u,Exp.}$ [kN]	$N_{u,F.E.}$ [kN]	$N_{u,F.E.}/N_{u,Exp.}$ [-]
CHS 6x3/16-SC1	69,045	234	152.18	4.85	399.43	0.641	0	576.65	549.08	0.95
CHS 6x3/16-SC2			152.05	4.84	399.01	0.970	0	540.38	550.21	1.02
CHS 6x3/16-e20-BC1			152.06	4.85	399.64	1.217	10.32	443.09	448.36	1.01
CHS 6x3/16-e20-BC2			152.12	4.86	399.75	0.978	14.27	425.23	426.56	1.00
CHS 6x3/16-e50-BC1[1]			152.11	4.82	448.79	0.444	59.28	232.60	276.51	1.19
CHS 6x3/16-e50-BC2			152.08	4.87	399.74	0.761	55.59	259.88	280.23	1.08
CHS 6x3/16-e70-BC1			152.10	4.88	398.88	0.873	94.40	202.34	205.43	1.02
CHS 6x3/16-e70-BC2[1]			152.15	4.89	399.45	0.926	92.40	182.88	208.41	1.14
CHS 8x1/8-SC1	65,549	276	202.67	3.24	598.67	0.860	0	481.68	522.78	1.09
CHS 8x1/8-SC2			202.56	3.26	598.82	1.182	0	489.05	520.01	1.06
CHS 8x1/8-e30-BC1			202.90	3.19	598.34	0.771	27.50	364.48	384.30	1.05
CHS 8x1/8-e30-BC2			202.96	3.20	598.70	1.321	29.12	375.52	380.85	1.01
CHS 8x1/8-e40-BC1			202.90	3.25	598.37	0.821	43.45	325.39	329.03	1.01
CHS 8x1/8-e40-BC2			202.96	3.20	598.82	1.026	42.60	314.45	320.03	1.02
CHS 8x1/8-e55-BC1			202.54	3.45	598.95	0.877	59.72	270.18	281.02	1.04
CHS 8x1/8-e55-BC2			202.54	3.45	599.00	0.960	56.03	281.76	296.05	1.05
									Mean	1.05
									C.O.V.	0.05

As a specific example, Figures 2 and 3 illustrate the comparison of test and numerical results for CHS 6x3/16 specimens. Figure 2 highlights the numerical model's capability to accurately capture not only the peak load but also the complete load-displacement response, encompassing several aspects such as (i) initial stiffness, (ii) peak load, and (iii) post-peak behavior. Figure 3 further compares failure shapes within the post-buckling range and shows similar patterns between the tested specimens and the F.E. simulations. Consequently, the F.E. models have consistently demonstrated their reliability and adequacy, justifying an extensive use for the subsequent parametric studies.

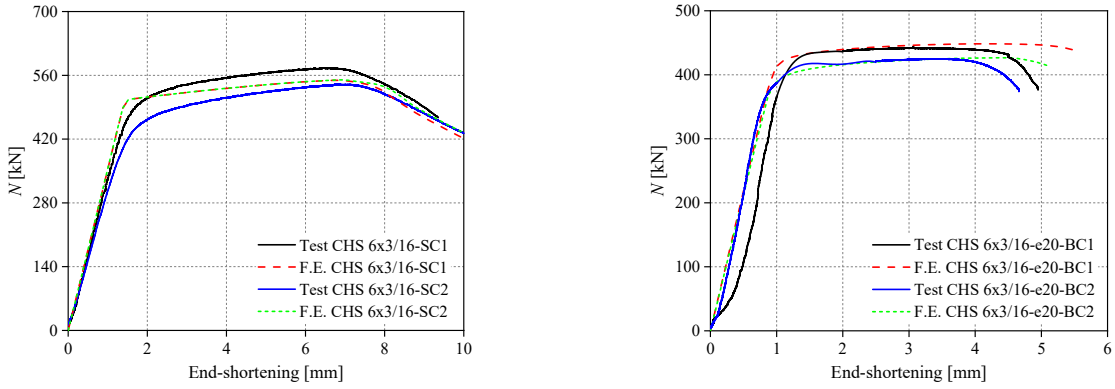

(**a**) (**b**)

Figure 2. Load-end shortening curves for CHS 6x3/16 specimens. (**a**) Stub columns tests. (**b**) Short beam-column tests.

(**a**) (**b**)

Figure 3. Typical failure modes for CHS 6x3/16 specimens. (**a**) CHS 6x3/16-SC2. (**b**) CHS 6x3/16-e20-BC1.

2.2. Parametric Studies

The validated F.E. models were used to conduct a series of parametric studies on the local buckling behavior of C.H.S. under axial compression N or pure bending moment M. The length of each numerical specimen was set to $3 \times D$, which is long enough for the effects of supports to remain negligible but short enough for the influence of member (global) buckling to be disregarded. Nodal forces, i.e., N or M, were applied at reference points (see Figure 1a,b) to create a compression load or a (constant) bending moment.

Furthermore, the lowest eigenmode shapes obtained from a linear bifurcation analysis (L.B.A.) were taken as initial local imperfection patterns and subsequently incorporated into G.M.N.I.A. analyses. In addition, to make sure the middle section of the "short element" remains the weakest one, odd numbers of half-waves have been chosen (see Figure 4).

(**a**) (**b**)

Figure 4. Typical elastic buckling modes (corresponding to lowest eigenvalues). (**a**) Under axial compression. (**b**) Under eccentric compression or pure bending.

Geometrical imperfections play a critical role in the local buckling behavior of C.H.S. and accurate characterization and consideration of geometrical imperfections are essential for the design of C.H.S. components. Therefore, a sub-study investigating the sensitivity of the numerical models to the magnitude of initial local imperfections ω_0 was conducted. Figure 5 displays the comparison between test and numerical results with various ω_0. Four sets of imperfection magnitude were investigated, including the measured value ω_{measured} [17], 0.1 t [21], $0.01\sqrt{Dt}$ [22], and $D/200$. As expected, when the specimens were more slender such as the CHS 8x1/8, it exhibited a greater sensitivity to variations in imperfection magnitude [23]. In comparison, the numerical results obtained with $\omega_0 = D/200$ are seen to be closer to the ones obtained with $\omega_0 = \omega_{\text{measured}}$. This imperfection magnitude provides greater accuracy and a higher level of safety. Therefore, it is advisable to consider $D/200$ as a reasonable value for local imperfection magnitudes in further parametric studies.

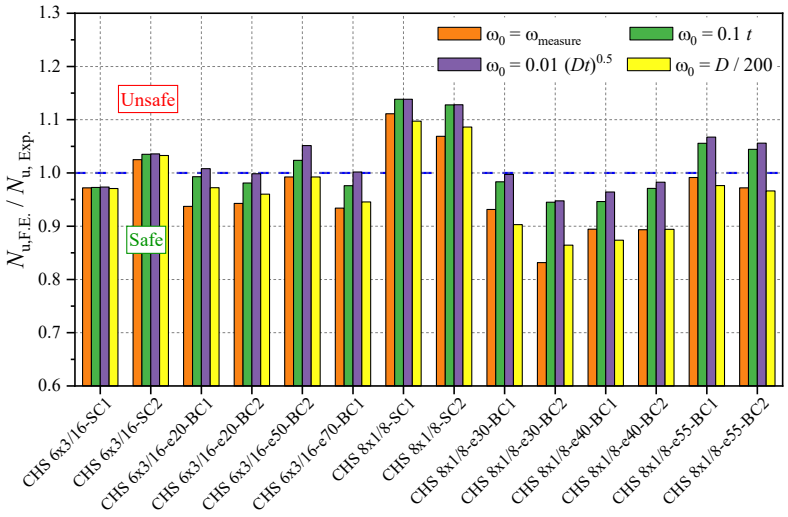

Figure 5. Comparison of test vs. F.E. results with various local imperfections' magnitudes.

A total of 126 simulations of G.M.N.I.A. have been performed for the C.H.S. under N or M. Moreover, 21 different geometries were selected, which include 17 geometries available in usual aluminum catalogues and four "invented cross sections" obtained with a decrease in the thickness t to extend the application range of the current study. The selected section geometries spanned from plastic (Class 1) to slender (Class 4) sections, defined in accordance with the slenderness limits provided in Eurocode 9 [8,9]. The D/t ratio of C.H.S. varied between 10.11 and 160.00, with D spanning from 19.05 to 177.80. For each section shape, three alloy types were considered, which include 6063-T6 with $\sigma_{0.2}$ = 170 MPa, 6081-T6 with $\sigma_{0.2}$ = 240 MPa, and 6082-T6 with

$\sigma_{0.2}$ = 260 MPa. The modified Ramberg-Osgood equation [24,25] was adopted to adequately represent the stress–strain relationships of these three aluminum alloys, as shown in Figure 6 [26].

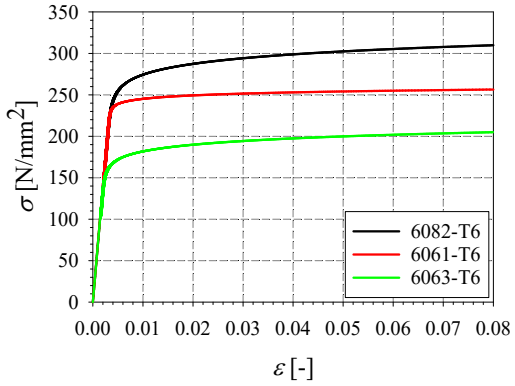

Figure 6. Stress–strain relationships for the various alloys considered [26].

3. Proposed Design Rules

Based on the F.E. results collected along the parametric studies, new design proposals for the C.H.S. under simple load cases were formulated, following the Overall Interaction Concept (O.I.C.) framework [27–32]. The O.I.C. framework is based on the well-established interaction between resistance and instability, and it effectively incorporates the effects of imperfections and their interactions with material yielding and buckling through $\overline{\lambda}_L - \chi_L$ buckling curves. The framework was developed with the aim of enhancing current design practice, improving accuracy, simplifying procedures, ensuring consistency, and providing a framework for computer-assisted resistance predictions.

The application steps of the O.I.C. are illustrated in Figure 7, highlighting three key load ratios: the plastic load ratio R_{pl}, the local elastic critical load ratio $R_{cr,L}$, and the ultimate resistance load ratio $R_{b,L}$. These ratios refer to the factors by which the initial loading needs to be multiplied to reach their respective limit cases. Note that two such ratios, R_{pl} and $R_{cr,L}$, can be calculated using approximate formulae suggested in current provisions [8,10] or by specific programs. In the present study, the HLS software [33] was adopted to determine R_{pl} and $R_{cr,L}$ for the full cross-section. After computing the cross-section slenderness $\overline{\lambda}_L$ via R_{pl} and $R_{cr,L}$, a local buckling reduction factor χ_L is determined using a local buckling curve, which leads to the calculation of the ultimate load ratio $R_{b,L}$. More information on the mechanical background of the O.I.C. can be found in [27].

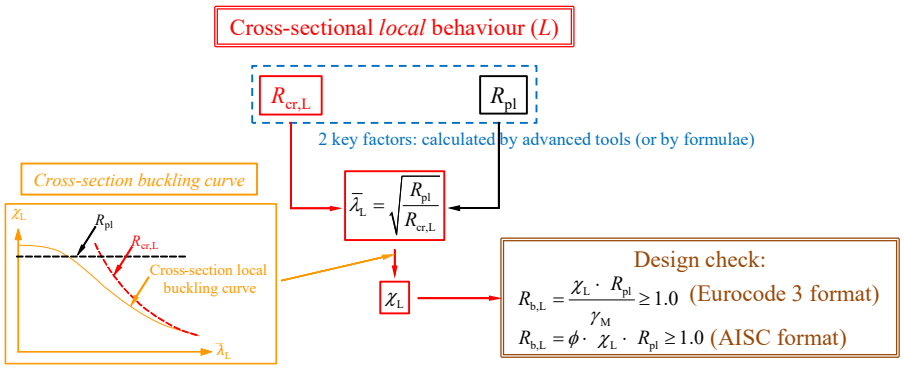

Figure 7. O.I.C. design flow chart for cross-section resistance.

The general $\overline{\lambda}_L - \chi_L$ format of O.I.C. was developed based on the well-known Ayrton–Perry approach [34,35] as defined by Equations (1) and (2), where λ_0 characterizes the length of a χ_L = 1.0 plateau, α_L considers the influence of imperfections, and δ accounts

for any post-buckling effects. Factor β captures possible strain hardening effects which may lead to a carrying capacity of the section slightly higher than the plastic resistance. All these factors were calibrated according to reference numerical results.

$$\chi_L = \frac{\beta}{\phi_L + \sqrt{\phi_L^2 - \lambda_L^{\delta} \cdot \beta}}, \tag{1}$$

$$\text{Where } \phi_L = 0.5 \cdot \left(1 + \alpha_L \cdot \left(\overline{\lambda}_L - \lambda_0\right) + \overline{\lambda}_L^{\delta} \cdot \beta\right), \tag{2}$$

Figure 8a,b present the numerical results obtained for C.H.S. sections under axial compression N and pure bending moment M, respectively, involving three different alloy types, i.e., 6063-T6, 6081-T6, and 6082-T6. Both figures present the influence of aluminum alloys on the cross-section resistance in the $\overline{\lambda}_L - \chi_L$ format of the O.I.C. framework. The horizontal axes represent the local slenderness of the section $\overline{\lambda}_L$, while vertical axes refer to the local buckling reduction coefficient χ_L.

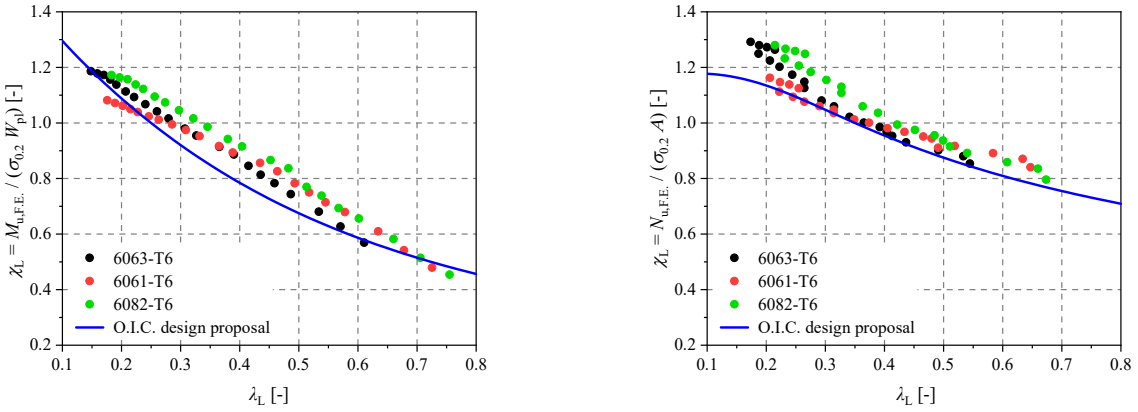

(**a**) (**b**)

Figure 8. Influence of different alloy types and O.I.C. local buckling curves. (**a**) C.H.S. under N. (**b**) C.H.S. under M.

For stocky sections with $\overline{\lambda}_L$ lower than λ_0, a clear tendency is observed. The sections made of 6082-T6 and 6063-T6 alloys exhibit higher nominal resistance χ_L compared to the sections made of 6061-T6. This difference can be attributed to the former two alloys benefiting more from strain-hardening effects when subjected to large strain levels. However, the results presented in Figure 8 indicate a relatively low influence of the alloy type on the overall outcome, confirming that the effect of material grade is adequately considered within the O.I.C. format. Therefore, based on these findings, it is accurate and economical to propose a single, safe-sided design curve for each load case. The proposed O.I.C. parameters for local buckling curves are summarized in Table 2 and relevant local buckling curves are illustrated in Figure 8.

Table 2. O.I.C. design procedure and factors for C.H.S. local buckling curves.

Load Case	λ_0	α_L	δ	β
N	0.35	0.32	0.40	1.0
M	0.25	1.45	1.45	1.0

Table 3 presents a comparison between F.E. results and analytical predictions for C.H.S. resistance capacity, including Eurocode 9 and the proposed O.I.C.-based design approach, applied to C.H.S. cross-sections under axial compression N or pure bending moment M. The ratio $\chi_{L+G,Ref.}/\chi_{L+G,F.E}$ represents the resistance predicted by two reference design

proposals in relation to the numerical results. If the ratio $\chi_{L+G,Ref.}/\chi_{L+G,F.E}$ is less than unity, it indicates that the predicted resistance is conservative. Conversely, if the ratio is greater than unity, it suggests that the design prediction is unconservative. Table 3 provides various statistical data regarding the $\chi_{L+G,Ref.}/\chi_{L+G,F.E}$. It includes the mean value, C.O.V., maximum value, minimum value, as well as the percentages of resistance predictions that are lower than 15% (conservative) on the safe side and higher than 5% and 10% (unconservative) on the unsafe side.

Table 3. Statistical results of $\chi_{L+G,Ref.}/\chi_{L+G,F.E}$ ratio for C.H.S under *N* or *M*.

Load Cases	Proposals	Mean	C.O.V.	Max.	Min.	<0.85 [%]	>1.05 [%]	>1.10 [%]
All	O.I.C.	0.939	0.051	1.060	0.827	1.6	0.8	0.0
	Eurocode 9	0.917	0.087	1.172	0.746	19.8	4.0	1.6
N	O.I.C.	0.945	0.040	1.005	0.865	0.0	0.0	0.0
	Eurocode 9	0.904	0.081	1.032	0.774	23.8	0.0	0.0
M	O.I.C.	0.932	0.059	1.060	0.827	3.2	1.6	0.0
	Eurocode 9	0.930	0.091	1.172	0.746	15.9	7.9	3.2

It is observed that the O.I.C. proposal performs better than the Eurocode 9 predictions for both compression and bending load cases. For all the cases studied in this paper, the mean values of the $\chi_{L+G,O.I.C.}/\chi_{L+G,F.E}$ ratio remain around 0.94 with a C.O.V. value as low as 0.05. In addition, over 91% of the predictions fall on the safe side, ensuring a reliable design approach. Furthermore, no O.I.C. prediction exceeds 1.06, indicating the reliability of the method without compromising safety. Considering these outcomes, the O.I.C. approach proves to be an excellent design proposal, providing more accurate, consistent, and safe resistance estimates compared to Eurocode 9. Its superior performance makes it a highly recommended choice for design applications.

4. Conclusions

This paper presented numerical investigations on circular hollow sections (C.H.S.) subjected to axial compression *N* or to pure bending moment *M*. The numerical models were validated against experimental results, confirming their ability to be substituted for physical tests. Parametric studies were then conducted to explore the local buckling behavior of C.H.S. with consideration of various alloy types and section geometries. Since geometrical imperfections play a critical role in the local buckling behavior of C.H.S., a sensitivity analysis was carried out to determine a reasonable local imperfections magnitude. It is recommended to adopt $D/200$ for further parametric studies. The results obtained from parametric studies were eventually used to validate an original design approach based on the Overall Interaction Concept (O.I.C.). The study revealed that sections made of 6082-T6 and 6063-T6 alloys exhibited higher nominal resistance compared to those made of 6061-T6, attributed to strain hardening effects. However, since the influence of alloy types on the overall outcome was relatively low, it was deemed accurate and economical to propose a single, safe-sided O.I.C.-based design curve for each load case. The O.I.C. proposal outperformed Eurocode 9 predictions for compression and pure bending load cases, indicating its superiority in terms of accuracy and reliability. Based on these findings, the O.I.C. approach is highly recommended for an improved, more economical design solution in aluminum C.H.S. applications.

Author Contributions: Conceptualization, L.L., N.B. and P.D.; methodology, L.L., N.B. and P.D.; software, L.L.; validation, L.L.; formal analysis, L.L.; investigation, L.L.; resources, L.L., S.D. and P.V.; data curation, L.L.; writing—original draft preparation, L.L.; writing—review and editing, L.L., P.V., N.B., P.D. and M.F.; visualization, L.L.; supervision, N.B. and M.F.; project administration, P.D., N.B. and M.F.; funding acquisition, P.D., N.B. and M.F. All authors have read and agreed to the published version of the manuscript.

Funding: This research was funded by Fonds de recherche du Québec (FRQNT)-FT131760.

Institutional Review Board Statement: Not applicable.

Informed Consent Statement: Not applicable.

Data Availability Statement: The data presented in this study are available on request from the corresponding author.

Acknowledgments: Special thanks to MAADI Group Inc. for providing the test specimens, to Denis Ouellet for his assistance in the scanner operations, and to Hugues Ferland for all the experimental investigations.

Conflicts of Interest: The authors declare no conflict of interest.

References

1. Beaulieu, D.; Marsh, C. *Design of Aluminum Structures*; Presses de l'aluminium: Saguenay, Canada, 2006.
2. Mazzolani, F. *Aluminium Alloy Structures*, 2nd ed.; E & FN Spon: London, UK, 1995.
3. Faella, C.; Mazzolani, F.M.; Piluso, V.; Rizzano, G. Local Buckling of Aluminum Members: Testing and Classification. *J. Struct. Eng.* **2000**, *126*, 353–360. [CrossRef]
4. Zhao, Y.; Zhai, X.; Wang, J. Buckling Behaviors and Ultimate Strengths of 6082-T6 Aluminum Alloy Columns under Eccentric Compression–Part I: Experiments and Finite Element Modeling. *Thin-Walled Struct.* **2019**, *143*, 106207. [CrossRef]
5. Zhao, Y.; Zhai, X.; Wang, J. Buckling Behaviors and Ultimate Strength of 6082-T6 Aluminum Alloy Columns with Square and Circular Hollow Sections under Eccentric Compression–Part II: Parametric Study, Design Provisions and Reliability Analysis. *Thin-Walled Struct.* **2019**, *143*, 106208. [CrossRef]
6. Wang, Z.X.; Wang, Y.Q.; Sojeong, J.; Ouyang, Y.W. Experimental Investigation and Parametric Analysis on Overall Buckling Behavior of Large-Section Aluminum Alloy Columns under Axial Compression. *Thin-Walled Struct.* **2018**, *122*, 585–596. [CrossRef]
7. Zhu, J.-H.; Young, B. Experimental Investigation of Aluminum Alloy Circular Hollow Section Columns. *Eng. Struct.* **2006**, *28*, 207–215. [CrossRef]
8. European Committee for Standardization. *Eurocode 9: Design of Aluminium Structures-Part 1-1: General Structural Rules*; Commission of the European Community: Brussels, Belgium, 2007.
9. European Committee for Standardization. *Eurocode 9: Design of Aluminium Structures-Part 1-5: Shell Structures*; Commission of the European Community: Brussels, Belgium, 2007.
10. The Aluminum Association. *'Aluminum Design Manual'*; The Aluminum Association: Washington, DC, USA, 2010.
11. *AS/NZS 1664.1:1997*; Aluminum Structures Part 1: Limit State Design. Standards Australia/Standards New Zealand: Sydney, Australia, 1997.
12. Zhu, J.-H.; Young, B. Numerical Investigation and Design of Aluminum Alloy Circular Hollow Section Columns. *Thin-Walled Struct.* **2008**, *46*, 1437–1449. [CrossRef]
13. Rong, B.; Zhang, Y.; Zhang, S.; Li, Z. Experiment and Numerical Investigation on the Buckling Behavior of 7A04-T6 Aluminum Alloy Columns under Eccentric Load. *J. Build. Eng.* **2022**, *45*, 103625. [CrossRef]
14. Zhao, Y.; Zhai, X. Bending Strength and Design Methods of the 6082-T6 Aluminum Alloy Beams with Circular Hollow Sections. *Structures* **2020**, *26*, 870–887. [CrossRef]
15. Zhu, J.-H.; Young, B. Aluminum Alloy Tubular Columns—Part II: Parametric Study and Design Using Direct Strength Method. *Thin-Walled Struct.* **2006**, *44*, 969–985. [CrossRef]
16. Wang, Y.; Fan, F.; Lin, S. Experimental Investigation on the Stability of Aluminium Alloy 6082 Circular Tubes in Axial Compression. *Thin-Walled Struct.* **2015**, *89*, 54–66. [CrossRef]
17. Li, L.; Dahboul, S.; Verma, P.; Dey, P.; Fafard, M.; Boissonnade, N. An Experimental Study on the Local Instability of Aluminium Circular Hollow Sections. In Proceedings of the CSCE Annual Conference, Moncton, NB, Canada, 24–27 May 2023.
18. *Abaqus Abaqus 6.11*; Dassault Systemes Simulia Corporation: Providence, RI, USA, 2011.
19. Zhou, F.; Young, B. Concrete-Filled Double-Skin Aluminum Circular Hollow Section Stub Columns. *Thin-Walled Struct.* **2018**, *133*, 141–152. [CrossRef]
20. Meng, X.; Gardner, L. Cross-Sectional Behaviour of Cold-Formed High Strength Steel Circular Hollow Sections. *Thin-Walled Struct.* **2020**, *156*, 106822. [CrossRef]
21. Buchanan, C.; Real, E.; Gardner, L. Testing, Simulation and Design of Cold-Formed Stainless Steel CHS Columns. *Thin-Walled Struct.* **2018**, *130*, 297–312. [CrossRef]
22. Meng, X.; Gardner, L. Simulation and Design of Semi-Compact Elliptical Hollow Sections. *Eng. Struct.* **2020**, *202*, 109807. [CrossRef]
23. Guo, L.; Liu, Y.; Jiao, H.; An, S. Behavior of Thin-Walled Circular Hollow Section Stub Columns under Axial Compression. *Int. J. Steel Struct.* **2016**, *16*, 777–787. [CrossRef]
24. Ramberg, W.; Osgood, W.R. *Description of Stress-Strain Curves by Three Parameters*; Technical Note No. 902; National Advisory Committee for Aeronautics: Washington, DC, USA, 1943.

25. Hill, H.N. *Determination of Stress-Strain Relations from "Offset" Yield Strength Values*; Technical Note No. 927; National Advisory Committee for Aeronautics: Washington, DC, USA, 1944.
26. Tristan, C. Development of an Alternative Design Method for Aluminium Open Cross-Sections Using the Overall Interaction Concept. Master's Thesis, Civil and Water Engineering Department, Laval University, Quebec City, QC, Canada, 2022.
27. Boissonnade, N.; Hayeck, M.; Saloumi, E.; Nseir, J. An Overall Interaction Concept for an Alternative Approach to Steel Members Design. *J. Constr. Steel Res.* **2017**, *135*, 199–212. [CrossRef]
28. Li, L.; Gérard, L.; Langlois, S.; Boissonnade, N. O.I.C.-Based Design of Mono-Symmetric I-Sections under Simple Load Cases. *Thin-Walled Struct.* **2022**, *174*, 109134. [CrossRef]
29. Li, L.; Gérard, L.; Kettler, M.; Boissonnade, N. The Overall Interaction Concept for the Design of Hot-Rolled and Welded I-Sections under Combined Loading. *Thin-Walled Struct.* **2022**, *172*, 108623. [CrossRef]
30. Li, L.; Fafard, M.; Boissonnade, N. Local and Global Instabilities of Rolled T-Section Columns under Axial Compression. *Thin-Walled Struct.* **2022**, *178*, 109517. [CrossRef]
31. Li, L.; Boissonnade, N. Local/Global Coupled Instabilities of Slender I-Sections under Compression. *Thin-Walled Struct.* **2022**, *172*, 108842. [CrossRef]
32. Gérard, L.; Li, L.; Kettler, M.; Boissonnade, N. Steel I-Sections Resistance under Compression or Bending by the Overall Interaction Concept. *J. Constr. Steel Res.* **2021**, *182*, 106644. [CrossRef]
33. Beyer, A.; Gardner, L.; Meng, X.; Taras, A. Reliability Assessment for the Generalized Slenderness Based Resistance Method for Circular and Elliptical Hollow Sections. *CE/Papers* **2021**, *4*, 2140–2148. [CrossRef]
34. Ayrton, W.E.; Perry, J. On Struts. *Engineer* **1886**, *62*, 513–515.
35. Maquoi, R.; Rondal, J. Mise En Équation Des Nouvelles Courbes Européennes de Flambement. *Constr. Métallique* **1978**, *15*, 17–30.